A Multiphysics Model of Lymph Node Hydraulics and Solute Transport with RTD-Based Validation

Presented by:

Riana Kandhai

Advisor:

Dr. Jacqueline Bridge

THE UNIVERSITY OF THE WEST INDIES
ST. AUGUSTINE CAMPUS

MPhil student, Department of Mechanical and Manufacturing Engineering

The University of the West Indies, St. Augustine Campus

Motivation & Gap

Lymph nodes (LNs):

Coordinate immune surveillance and lymph transport

Encounter difficulty measuring node-scale hydraulics and solute residence times in vivo

Provide an integrated, validated model linking free-flow sinuses, porous parenchyma, and tissue mechanics to solute dynamics

Objectives

- Develop 2D axisymmetric COMSOL model of a single lymph node
- Couple Stokes (sinuses), Darcy/Brinkman (parenchyma), and linear Biot poroelasticity (tissue)
- Simulate passive solute advection–diffusion and compute residence-time distribution (RTD)
- Calibrate medullary permeability and validate transnodal pressure drop ($\Delta p \approx 1$ mmHg)

Model Overview — Physics & Interfaces (COMSOL)

Free-flow sinuses & ducts

- Solve incompressible laminar flow in the Stokes limit at low Re
- Apply no-slip on capsule and ducts; set outlet static pressure

Parenchyma

- Solve Darcy/Brinkman with **superficial** velocity formulation
- Enforce continuity of pressure and normal flux at sinus–core interfaces

Tissue

- Couple pore pressure and solid displacement via linear Biot poroelasticity
- Use Darcy flux equal to the superficial velocity in the porous region

Species

- Advect and diffuse a passive tracer in free and porous media
- Accumulate by void fraction $\varepsilon$with $\varepsilon = 1$in free flow and $\varepsilon = \phi$in porous media

Multiphysics couplings

- Couple Free and Porous Media Flow for momentum transfer across interfaces
- Couple Poroelasticity for tissue–fluid interaction

Geometry & Domains (2D Axisymmetric)

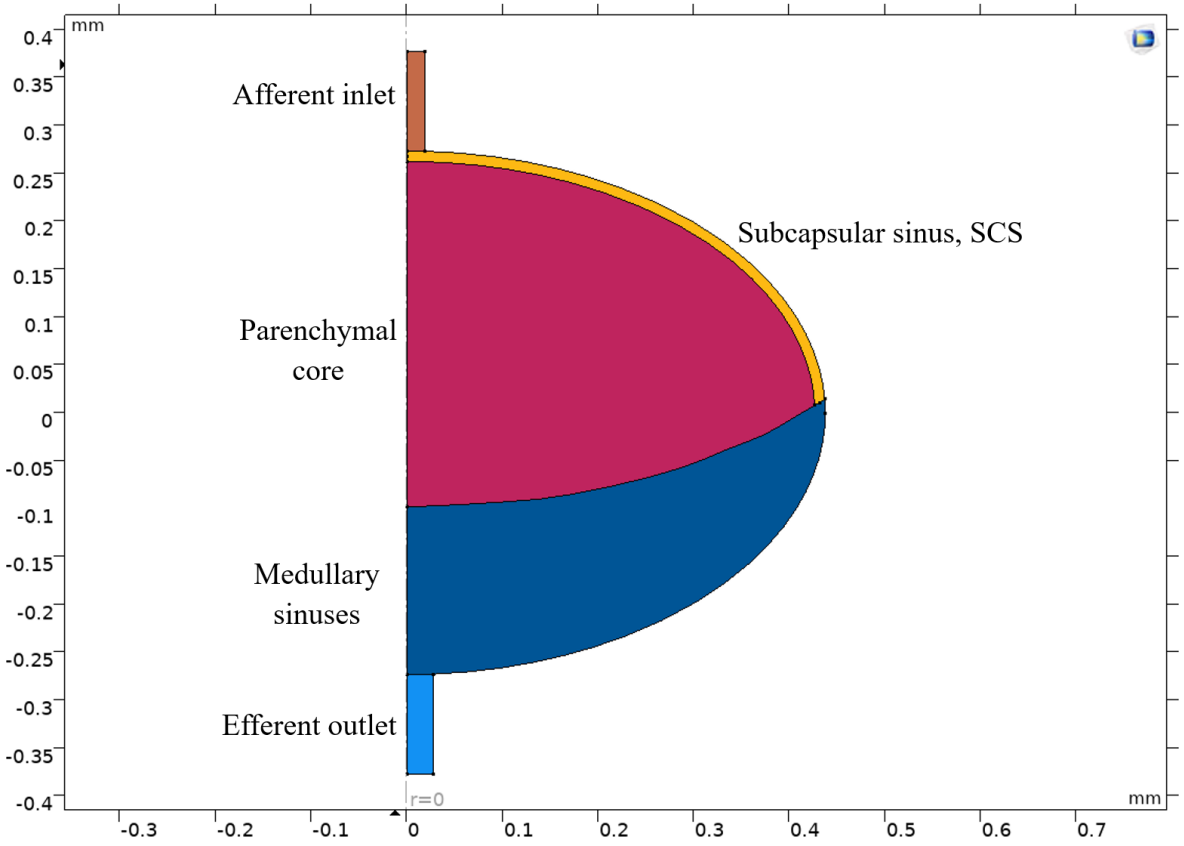

Figure 1. 2D axisymmetric lymph-node geometry and domains. The subcapsular sinus (SCS) and medullary sinuses are modeled as free-flow regions; the central parenchymal core is porous; short afferent and efferent ducts are included. The left vertical line is the symmetry axis $r = 0$.

Free flow (sinuses/ducts)

- Enforce continuity $\nabla \cdot \mathbf{u} = 0$
- Solve $\rho\left(\frac{\partial \mathbf{u}}{\partial t} + \mathbf{u} \cdot \nabla \mathbf{u}\right) = -\nabla p + \mu \nabla^2 \mathbf{u}$ (Stokes limit at low Re)

Porous

- Apply Darcy Law $\mathbf{u} = -\frac{\kappa}{\mu}(\nabla p - \rho \mathbf{g})$
- Solve $-\nabla p + \mu \nabla^2 \mathbf{u} - \frac{\mu}{\kappa}\mathbf{u} + p\mathbf{g} = 0$ (Brinkman)

Poroelastic

- Use linear Biot with effective stress σ′, Biot coefficient α, specific storage S
- Solve $\nabla \cdot \boldsymbol{\sigma}' - \alpha \nabla p + \rho_s \mathbf{b} = 0$
- Solve $S\frac{\partial p}{\partial t} + \alpha \frac{\partial}{\partial t}(\nabla \cdot \mathbf{u}_s) + \nabla \cdot \mathbf{u} = 0$

Transport

- Solve $\frac{\partial(\varepsilon c)}{\partial t} + \nabla \cdot (\mathbf{u}c) = \nabla \cdot \left(\varepsilon D_{eff} \nabla c\right) + R(c)$, with ε=1 (free flow), ε=ϕ (porous media).

Governing Equations

SYMBOL	QUANTITY
$\mathbf{u}$	Velocity
p	Pressure
μ	Viscosity
ρ	Density
κ	Permeability
$\mathbf{g}$	Gravity
$\boldsymbol{\sigma}'$	Effective stress
α	Biot coefficient
S	Specific storage
$\mathbf{u}_s$	Solid displacement
ε	Void fraction
ϕ	Porosity
D_{eff}	Effective diffusivity
$R(c)$	Reaction term

Boundary & Initial Conditions

Inlet

- Apply Q_{in} = 0.01 $mL \cdot h^{-1}$ (2.78×10^{-12} $m^3 \cdot s^{-1}$) over afferent windows
- Single-inlet geometry $Q_{in,tot} = Q_{in}$

Walls & Outlet

- Set internal walls to no-slip
- Set outlet static pressure $p_{out} = 466.6Pa \approx 3.5mmHg$

Transport (RTD)

- Impose 10 s top-hat tracer pulse at inlet
- Treat walls as no-flux; use convective-flux outlet

Initialisation

- Use stationary hydraulic solution to seed transient transport

Mesh & Numerical Verification

Mesh construction

- Use unstructured triangles with boundary-layer (BL) rows along capsule/SCS and ducts
- Grade elements across sinus–parenchyma interfaces (growth ≤ 1.1; ≥ 3 BL rows)

Mesh set

- Generate meshes M1–M3 with progressive refinement

Verification metrics

- Track Δp, Q_{out}, shunting fraction, and mean RTD across M1–M3

Mesh independence

- Declare independent: Δp < 1%, Q_{out} < 0.1%, shunting < 0.5 percentage points, mean RTD < 2% from M2 to M3

Methods — RTD Protocol

- $S(t) = c_{out}(t)Q_{out}(t)$ [effluent signal]
- $E(t) = \frac{S(t)}{M_{in}}$, with $M_{in} = \int c_{in}(t)Q_{in}(t)dt$
- Check mass recovery $\int_0^\infty E(t)dt \approx 1$

  - $F(t) = \int_0^t E(\tau)d\tau$ (cumulative)
  - $\bar{t} = \int_0^\infty tE(t)dt$ (mean residence time)

✓ Integrate geometry, permeability, and flow partitioning into a single observable via $E(t)$, $F(t)$, and $\bar{t}$

✓ Calibrate porous parameters and validate targets (e.g., Δp)

Calibration & Validation Targets

1

Calibrate transnodal pressure drop $\Delta p \approx 1$ mmHg under physiologic inflow

2

Confirm dominant peripheral shunting through SCS/medullary pathway (>90%)

3

Check subcapsular sinus velocities and capsule wall shear stress fall within plausible ranges

Results — Pressure Field & Δp

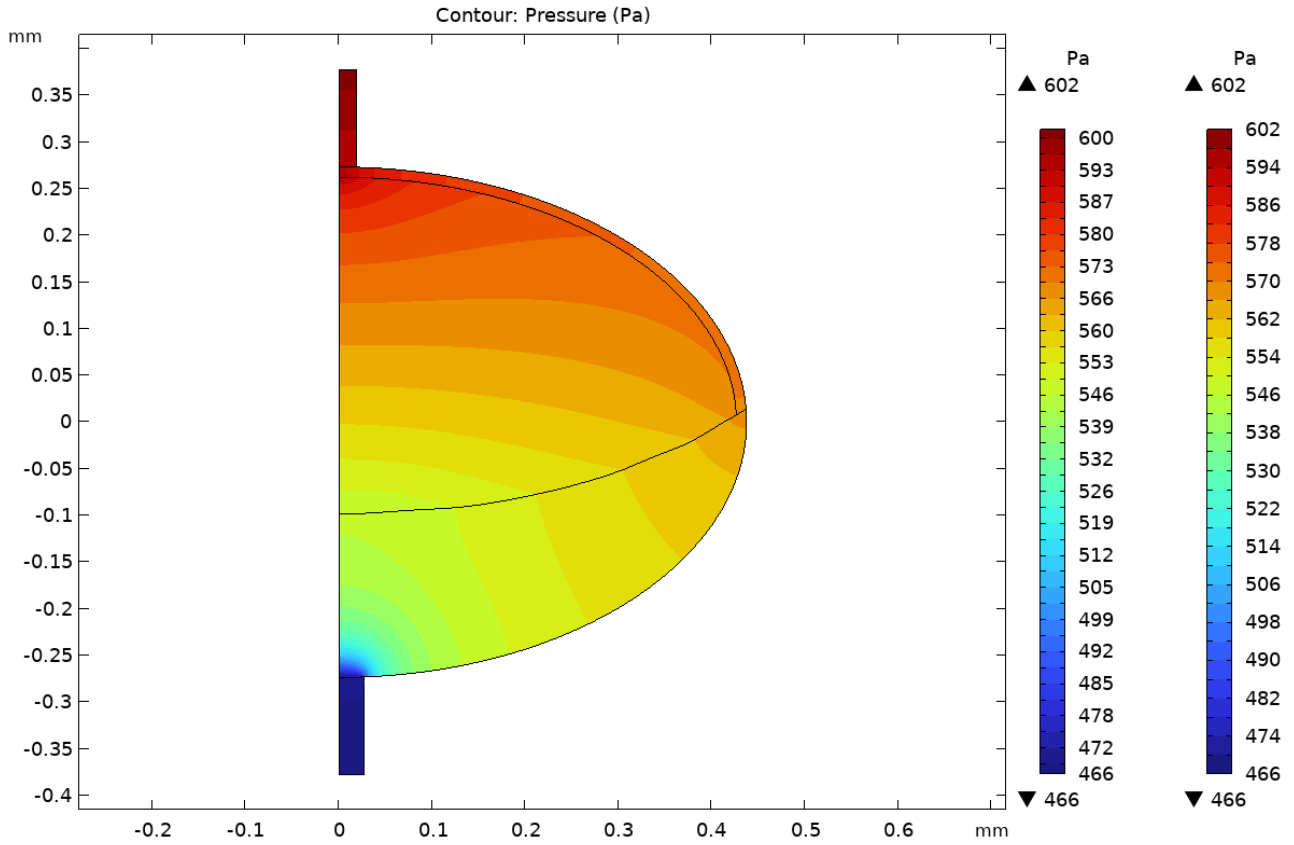

Figure 2. Pressure field and transnodal drop. Contours of static pressure p(Pa) in the 2D axisymmetric model; $p_{in} \approx 600.5\ Pa$, $p_{out} = 466.6\ Pa$. The transnodal pressure drop is $\Delta p \approx 133.8\ Pa (\approx 1.00\ mmHg)$; mass balance holds ($Q_{in} = Q_{out}$).

Report peripheral routing fraction ≈99.9% via SCS/medullary sinuses

Observe minor core perfusion, consistent with mouse LN models (~90% peripheral)

Infer geometry and permeability dominate routing at ~mmHg transnodal drops

Results — Flow Partition (Peripheral Shunting)

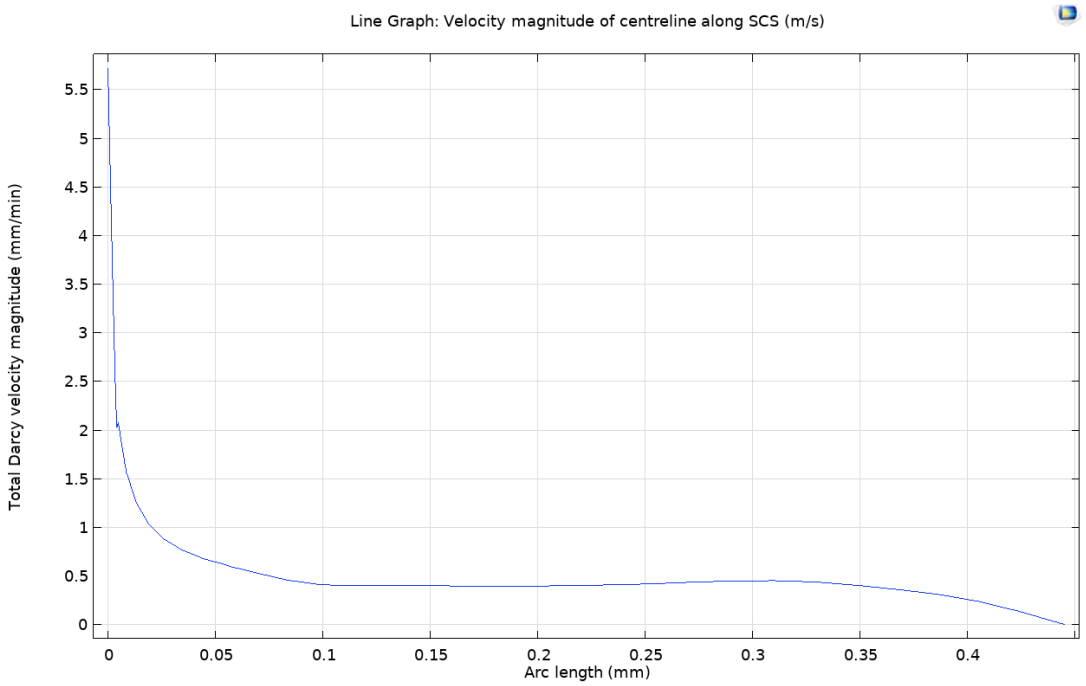

Figure 3. SCS centreline velocity vs. arc length (mm·min^{-1}). Arc length s was measured along the capsule/SCS midline from the afferent entry (s=0) toward the hilum; the centreline was sampled at the SCS mid-thickness.

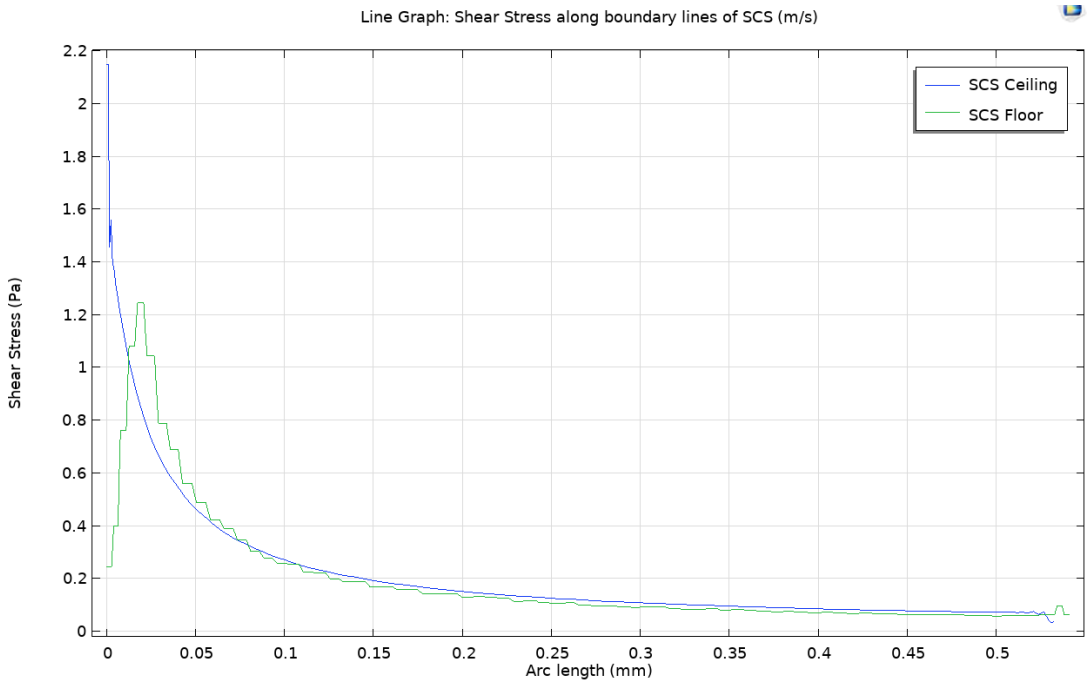

Figure 4. Capsule/SCS wall shear stress vs. arc length (Pa; ceiling & floor)

Results — SCS Velocity & Capsule Shear

Results — Interstitial (Parenchymal) Pressure

Report mean parenchymal (porous) pressure ≈ 562 Pa (≈ 4.22 mmHg)

Map spatial range ≈ 3.50–4.46 mmHg, consistent with outlet = 3.50 mmHg and Δp ≈ 1 mmHg

Align with in vivo absolute scales reported for murine LNs

Results — Species Transport (T, B, Other)

Figure 5. Species concentration fields with total-flux streamlines at 60 s (left) and 600 s (right). Top: T-cells; middle: B-cells; bottom: Other Leukocytes.

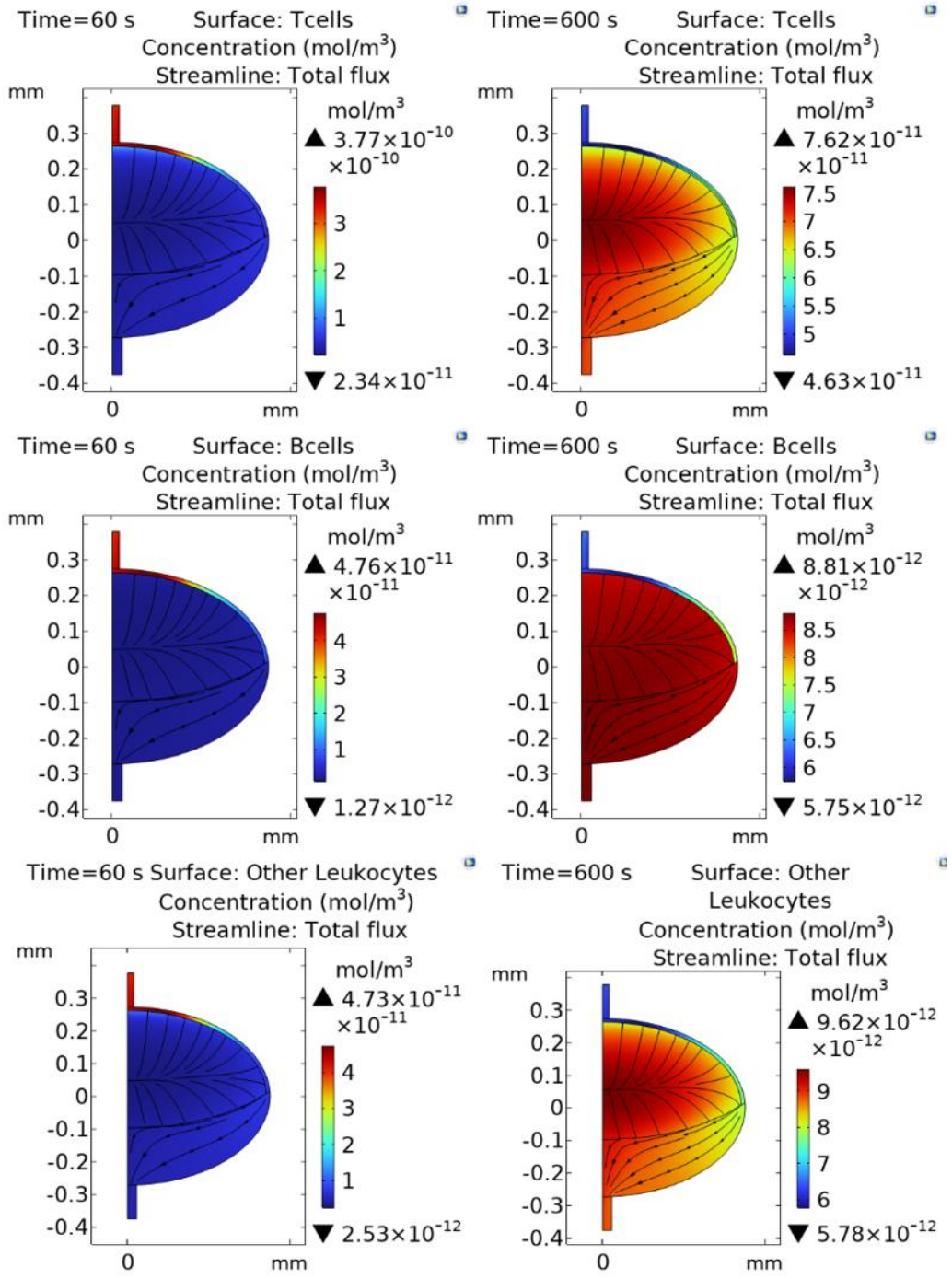

Results – Species Transport (T-cells, B-cells, Other Leukocytes)

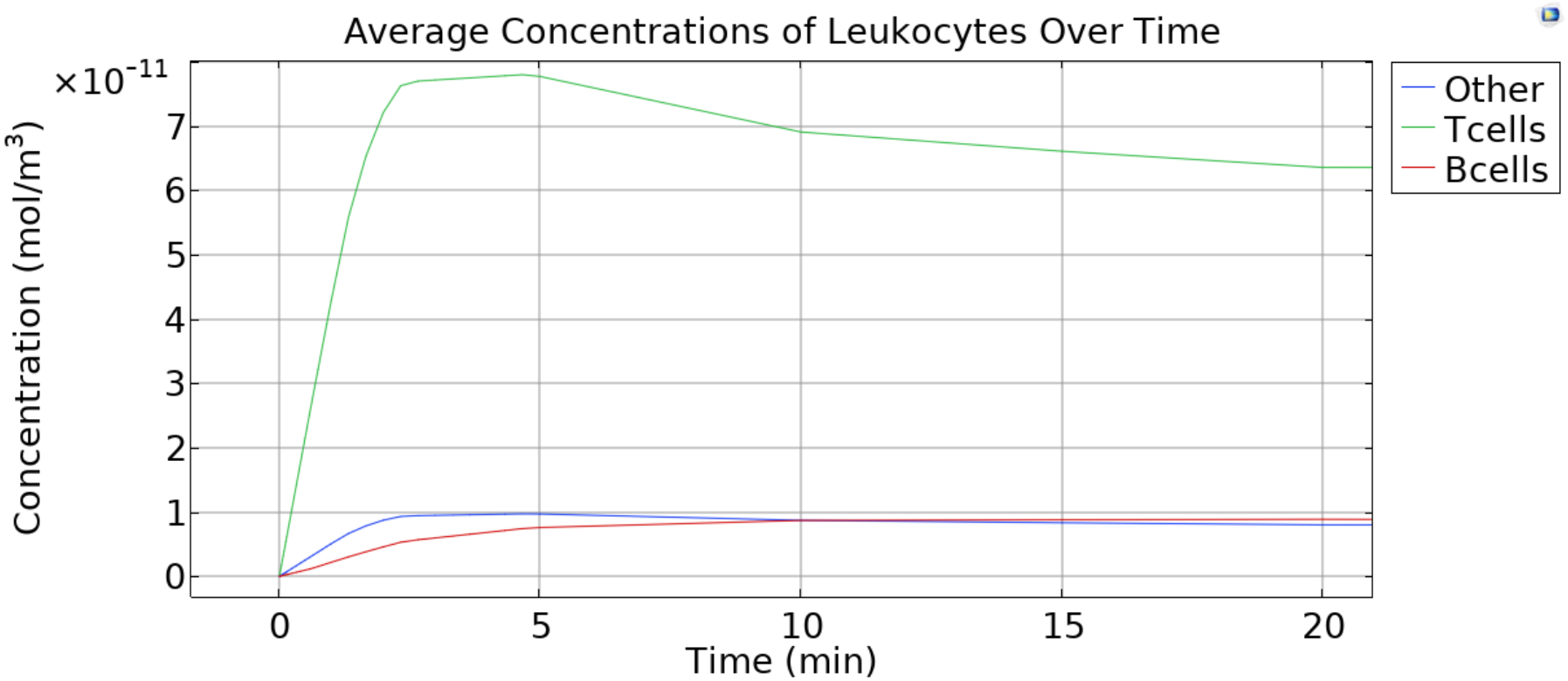

Figure 6. Volume-averaged concentration $\bar{c}(t)$ over the whole node (free + porous) for three species with distinct D_{eff}. Inlet top-hat pulse at $t = 0$ for 10 s; curves show $\bar{c}(t)$ for T-cells, B-cells, and Other Leukocytes over 0–20 mins.

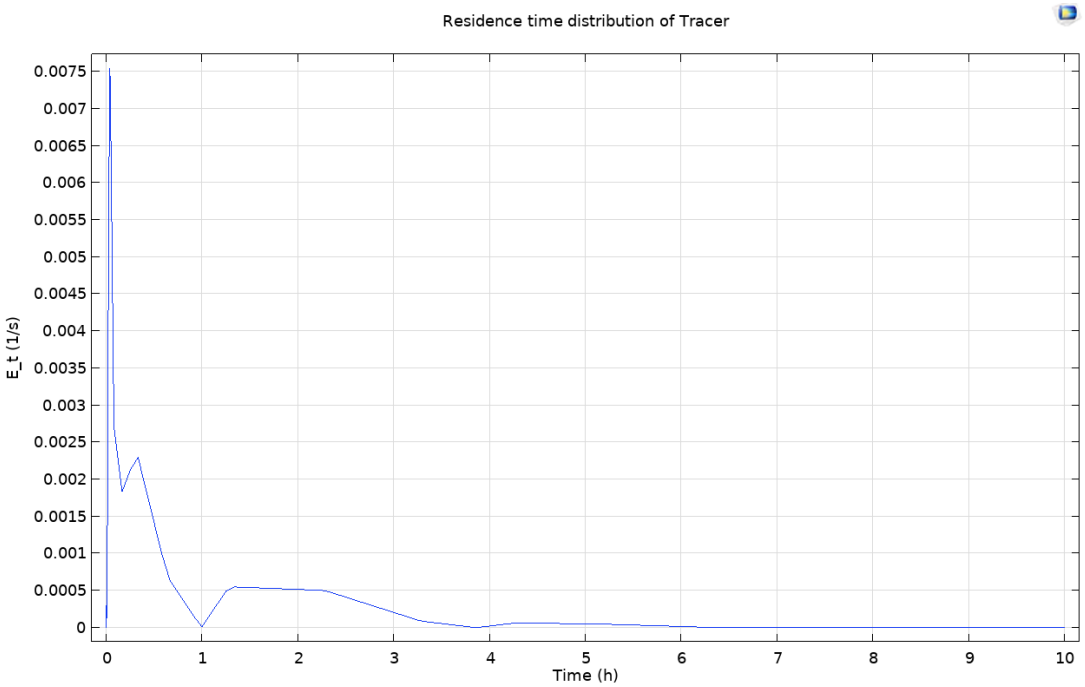

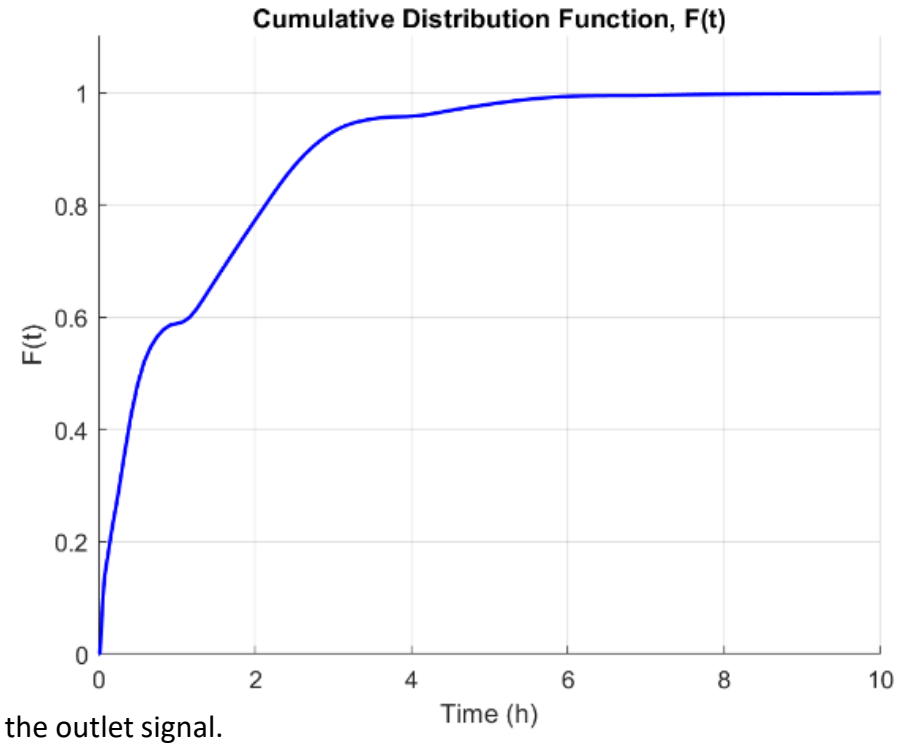

Residence-time distribution from the outlet signal.

Figure 7. $E(t) = C_{out}(t)Q_{out}(t)/M_{in}$with $\int_0^\infty E\,(t)\,dt \approx 1$;mean residence time $\tau \approx 3.98\ h$.

Figure 8. Cumulative $F(t) = \int_0^t E\,(\tau)\,d\tau$)dimensionless).

Results – RTD (E(t) & F(t))

Limitations

01

Restrict to 2D axisymmetry; omit valves, pulsatility, and explicit microvascular exchange

02

Initialize transient transport from steady hydraulics, which can accentuate peripheral shunting

03

Extend to 3D geometry, pulsatile inflow and valves, explicit blood–lymph exchange, and spatial heterogeneity

Conclusions & Outlook

Match transnodal pressure drop Δp ≈ 1 mmHg and near-unity peripheral routing

Provide quantitative metrics

Δp, wall shear stress, interstitial pressure p, shunting fraction, RTD

Enable mechanistic extensions

chemokines/cell transport, heterogeneity, 3D geometry, valves

Appendix – Table 1 (Model Inputs)

Category	Quantity	Symbol	Baseline	Units
Geometry (axisymmetric)	Outer ellipse semi-axis (radial)	a_{out}	0.80	mm
	Outer ellipse semi-axis (axial)	b_{out}	0.50	mm
	SCS inner ellipse semi-axis (radial)	$a_{SCS,in}$	0.79	mm
	SCS inner ellipse semi-axis (axial)	$b_{SCS,in}$	0.49	mm
	Parenchyma ellipse semi-axis (radial)	a_{core}	0.78	mm
	Parenchyma ellipse semi-axis (axial)	b_{core}	0.48	mm
	SCS nominal thickness (radial/axial)	t_{SCS}	0.01	mm
	Afferent window width	w_{aff}	0.07	mm
	Afferent window height	h_{aff}	0.20	mm
	Efferent window width	w_{eff}	0.10	mm
	Efferent window height	h_{eff}	0.20	mm
Fluid (free-flow: SCS/EF/AF)	Density	ρ	1040	$kg \cdot m^{-3}$
	Dynamic viscosity	μ	1.2×10^{-3}	$Pa \cdot s$
Fluid in porous regions (Darcy)	Density	ρ	1000	$kg \cdot m^{-3}$
	Dynamic viscosity	μ	1.2×10^{-3}	$Pa \cdot s$
Porous matrix - TC (parenchyma)	Porosity	Φ	0.30	—
	Intrinsic permeability	κ	7.6×10^{-17}	m^2
	Young's modulus (drained)	E	2×10^{3}	Pa
	Poisson's ratio	ν	0.35	—
Porous matrix — MS (medullary)	Porosity	Φ	0.65	—
	Intrinsic permeability	κ	4.85×10^{-13}	m^2
	Young's modulus (drained)	E	1200	Pa
	Poisson's ratio	ν	0.35	—
Poroelastic coupling	Biot–Willis coefficient	α_B	0.8	—
Free-flow BCs	Inlet (afferent)	—	2.7778×10^{-12}	$m^3 \cdot s^{-1}$
	Outlet pressure (efferent)	p_{out}	466.6	Pa
Species (solutes)	Diffusivity — small tracer	D_{small}	4.6×10^{-10}	$m^2 \cdot s^{-1}$
Species (cells)	Fluid diffusion — T cells	D_T	1.1×10^{-12} (≈67 μm²/min)	$m^2 \cdot s^{-1}$ (μm²/min)
	Fluid diffusion — B cells	D_B	2.0×10^{-13} (≈12 μm²/min)	$m^2 \cdot s^{-1}$ (μm²/min)
	Fluid diffusion — other leukocytes (non-B, non-T; e.g., NK, dendritic)	D_{other}	5.0×10^{-13} (≈30 μm²/min)	$m^2 \cdot s^{-1}$ (μm²/min)
	Concentration — T cells	c_T	6.64×10^{-11}	$mol \cdot m^{-3}$
	Concentration — B cells	c_B	8.3×10^{-12}	$mol \cdot m^{-3}$
	Concentration — other leukocytes (non-B, non-T)	c_{other}	8.3×10^{-12}	$mol \cdot m^{-3}$
Axisymmetry	Swirl velocity	u_θ	0	—
RTD (transient tracer)	Pulse duration	t_p	10	s
	Pulse magnitude	c_0	8.3×10^{-12}	$mol \cdot m^{-3}$

References

[1] M. J. Davis, S. D. Zawieja and P. D. King, “Transport and Immune Functions of the Lymphatic System,” *Annual Review of Physiology,* vol. 87, no. 1, p. 151–172, 2025.

[2] L. Li, J. Wu, R. Abdi, C. M. Jewell and J. S. Bromberg, “Lymph Node Fibroblastic Reticular Cells Steer Immune Responses,” *Trends in Immunology,* vol. 42, no. 8, p. 723–734, 2021.

[3] A. Takeda, M. Salmi and S. Jalkanen, “Lymph Node Lymphatic Endothelial Cells as Multifaceted Gatekeepers in the Immune System,” *Trends in Immunology,* vol. 44, no. 1, p. 72–86, 2023.

[4] K. Maisel, C. A. McClain, A. Bogseth and S. N. Thomas, “Nanotechnologies for Physiology-Informed Drug Delivery to the Lymphatic System,” *Annual Review of Biomedical Engineering,* vol. 25, p. 233–256, 2023.

[5] M. Jafarnejad, M. R. Woodruff, P. S. Zawieja, J. B. Carroll and J. E. J. Moore, “Modeling Lymph Flow and Fluid Exchange with Blood Vessels in Lymph Nodes,” *Lymphatic Research and Biology,* vol. 13, no. 4, p. 234–247, 2015.

[6] G. Giantesio, A. Girelli and A. Musesti, “A Model of the Pulsatile Fluid Flow in the Lymph Node,” *Mechanics Research Communications,* vol. 116, p. 103743, 2021.

[7] A. Girelli, G. Giantesio, A. Musesti and R. Penta, “Multiscale Computational Analysis of the Steady Fluid Flow through a Lymph Node,” *Biomechanics and Modeling in Mechanobiology,* vol. 23, p. 2005–2023, 2024.

[8] T. D. Jayathungage Don, S. Safaei, G. D. Maso Talou, P. S. Russell, A. R. J. Phillips and H. M. Reynolds, “Computational Fluid Dynamic Modeling of the Lymphatic System: A Review of Existing Models and Future Directions,” *Biomechanics and Modeling in Mechanobiology,* vol. 23, no. 1, p. 3–22, 2024.

[9] F. P. Assen, J. Abe, M. Hons, R. Hauschild, S. Shamipour, W. A. Kaufmann, T. Costanzo and e. al., “Multitier Mechanics Control Stromal Adaptations in Swelling Lymph Nodes,” *Nature Immunology,* vol. 23, no. 8, p. 1246–1255, 2022.

[10] A. E. Rodrigues, “Residence time distribution (RTD) revisited,” *Chemical Engineering Science,* vol. 230, p. 116188, 2021.

[11] M. Hwang, J. Wang and S. Jung, “Understanding the Residence Time Distribution in a Transient Inline Spiking System: Modeling, Experiments, and Simulations,” *Membranes,* vol. 13, p. 375, 2023.

[12] L. C. Dieterich, C. Tacconi, L. Ducoli and M. Detmar, “Lymphatic vessels in cancer,” *Physiological Reviews,* vol. 102, no. 4, p. 1837–1879, 2022.

References

[13] R. L. Panton, Incompressible Flow, Hoboken, NJ: Wiley, 2013.

[14] D. A. Nield and A. Bejan, Convection in Porous Media, Cham: Springer, 2017.

[15] O. Coussy, Poromechanics, Hoboken, NJ: Wiley, 2004.

[16] A. H.-D. Cheng, Poroelasticity, Cham: Springer, 2016.

[17] M. Dentz, J. J. Hidalgo and D. Lester, "Mixing in Porous Media: Concepts and Approaches Across Scales," *Transport in Porous Media,* vol. 146, no. 1, p. 5–53, 2023.

[18] N. L. Browse, R. L. Doig and D. Sizeland, "The Resistance of a Lymph Node to Lymph Flow," *British Journal of Surgery,* vol. 71, no. 3, p. 192–196, 1984.

[19] G. Giantesio, A. Girelli and A. Musesti, "A Mathematical Description of the Flow in a Spherical Lymph Node," *Bulletin of Mathematical Biology,* vol. 84, p. 142, 2022.

[20] J. A. Kornuta, Z. Nepiyushchikh, O. Y. Gasheva, A. Mukherjee, D. C. Zawieja and J. B. Dixon, "Effects of dynamic shear and transmural pressure on wall shear stress sensitivity in collecting lymphatic vessels," *American Journal of Physiology–Regulatory, Integrative and Comparative Physiology,* vol. 309, no. 9, p. R1122–R1134, 2015.

[21] J. E. J. Moore and C. D. Bertram, "Lymphatic System Flows," *Annual Review of Fluid Mechanics,* vol. 50, no. 1, p. 459–482, 2018.

[22] E. M. Bouta, R. W. Wood, E. B. Brown, H. Rahimi, C. T. Ritchlin and E. M. Schwarz, "In vivo quantification of lymph viscosity and pressure in lymphatic vessels and draining lymph nodes of arthritic joints in mice," *The Journal of Physiology,* vol. 592, no. 6, pp. 1213-1223, 2014.

[23] C. C. Clement, W. Wang, M. Dzieciatkowska, M. Cortese, K. C. Hansen, A. Becerra, S. Thangaswamy, I. Nizamutdinova, J.-Y. Moon, L. J. Stern, A. A. Gashev, D. Zawieja and L. Santambrogio, "Quantitative Profiling of the Lymph Node Clearance Capacity," *Scientific Reports,* vol. 8, no. 1, p. 11253, 2018.

Thank you!

A Multiphysics Model of Lymph Node Hydraulics and Solute Transport with RTD-Based Validation

Presented by:

Riana Kandhai

riana.kandhai@my.uwi.edu

Advisor:

Dr. Jacqueline Bridge

MPhil student, Department of Mechanical and Manufacturing Engineering

The University of the West Indies, St. Augustine Campus

THE UNIVERSITY
OF THE
WEST INDIES
ST. AUGUSTINE CAMPUS